Continuous-mode laser ablation at the solid-liquid interface of pelletized low-cost materials for the production of luminescent silicon carbide nanocrystals

M. Carmen Ortega-Liébana[#,†], José L. Hueso[#,†,], Raul Arenal[‡,&], Ruth Lahoz[§], Germán F. de la Fuente[§,*] and Jesús Santamaría[#,†]*

[#]Institute of Nanoscience of Aragon (INA) and Department of Chemical Engineering and Environmental Technology, University of Zaragoza, Zaragoza, 50018, Spain.

[†]CIBER de Bioingeniería, Biomateriales y Nanomedicina, CIBER-BBN, Zaragoza, 50018, Spain.

[‡]Laboratorio de Microscopias Avanzadas (LMA), Instituto de Nanociencia de Aragon (INA), Universidad de Zaragoza, Zaragoza, 50018, Spain.

[&]ARAID Foundation, Zaragoza, 50018, Spain.

[§]Institute of Materials Science of Aragón (ICMA), CSIC-University of Zaragoza, Zaragoza, 50018, Spain.

We report on the fabrication of silicon carbide (SiC) nanocrystals using a continuous scanning mode laser for the ablation of pelletized SiC microparticles (NPs). As a major advantage, we propose the *in-situ* generation and collection of freestanding nanoparticles in an ethanol liquid media and the use of cost-effective SiC targets in comparison with those commercially available or synthesized after multiple-steps. The SiC NPs exhibit luminescent properties under UV exposure and excellent colloidal stability for extended periods of time. The influence of a more oxidizing solvent such as water is also evaluated as collecting media.

TOC GRAPHICS

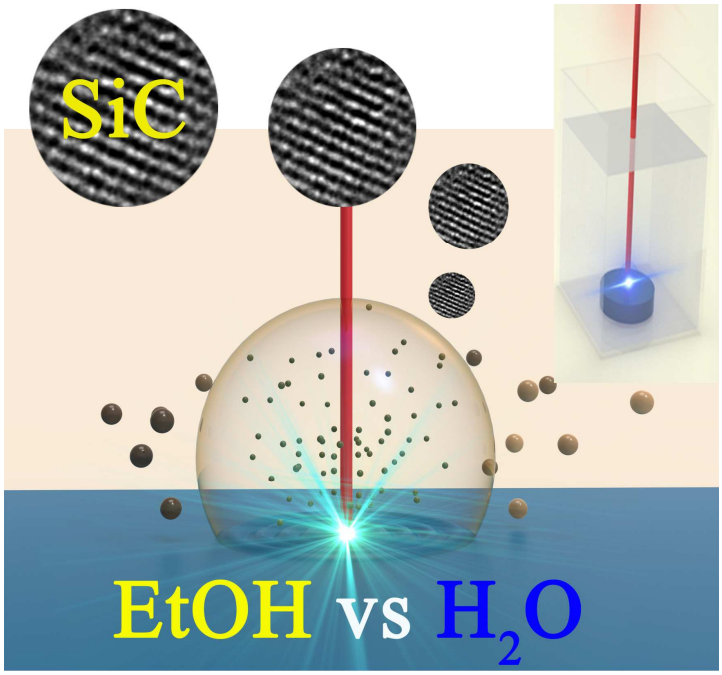

KEYWORDS. Quantum dots, plasmas, laser, EELS, nanoparticles, micro-powdered SiC

The synthesis and properties of silicon carbide nanoparticles (SiC NPs) and other group IV elements have attracted great interest in the past few years [1]. SiC is a semiconductor material with a wide range of applications due to its high thermal conductivity, chemical stability, wide band gap and high hardness. It has been demonstrated that after downsizing the SiC dimensions to the nanoscale level, quantum confinement effects provide this semiconductor with photo-luminescent properties not observed in the bulk counterpart [2-6]. Therefore, the synthesis of luminescent SiC NPs has boosted novel research fields of interest such as the fabrication of next-generation optical nanodevices or the use as labels for bioimaging and diagnostics [7]. The intrinsic biocompatibility and chemical stability of SiC represents a serious advantage for bioimaging applications in comparison with other light-emitting quantum dots containing toxic heavy metals or silicon nanocrystals requiring surface passivation to maintain their stability [8]. Moreover, their improved resistance to photo-bleaching, size-dependent absorption and emission, as well as broad absorption spectra and narrow emission spectra, makes the SiC NPs a better option than other fluorescent dyes.

Photoluminescence (PL) emission properties of SiC nanocrystals are strongly dependent on the fabrication methods that may affect the number of interior defects formed and the surface-bonding structures. In recent years, different strategies have been exploited for the synthesis of freestanding SiC NPs [9]. Among the chemical methods, it is worth mentioning the carbo-thermal reduction[10], sol-gel processing[11] and wet-chemical etching of bulk SiC assisted by electrode anodization[2-3] or in electroless configurations[4]. Laser pyrolysis[12-13] and laser ablation[14-15] represent the most widespread physical approaches. Both laser methodologies have traditionally faced certain drawbacks associated with the lack of size and composition

control[16] that have been recently overcome with the use of high intensity NIR and UV emitting lasers and the addition of liquid solvents to collect and stabilize the freestanding NPs[16-23].

Recently, laser ablation synthesis in liquid solution[16,24] (LASiS) has been preferentially selected for the production of luminescent SiC NPs due to its simplicity, environmental friendliness and extreme non-equilibrium local conditions[23,25]. Moreover, LASiS represents a promising approach for the scalable production of bulk quantities of SiC NPs within the nanoscale regime, which remains as an open challenge. Although SiC targets for laser ablation can be synthesized from various precursors, such as polycrystalline wafers[23,25] or rods, they are both time-consuming and difficult to prepare/handle or can generate a combination of different Si-based species that require post-treatment [25]. In this work, we report a simple, straight-forward and cost-effective method to prepare freestanding SiC NPs with mean sizes below 10 nm by laser ablation of inexpensive pelletized SiC micro-powder targets. The influence of using an aqueous or an organic dispersing media is also evaluated and discussed. Moreover, the use of a continuous wave laser with uniform scanning mode is presented as an effective alternative to more expensive and energetic laser sources working at shorter frequencies.

Synthesis of SiC nanoparticles by laser ablation in aqueous and alcoholic solvents. The SiC NPs were synthesized by laser ablation of pelletized SiC powders previously immersed in a glass vessel containing 10 mL of either doubly de-ionized water (DDI-H_2O) or absolute ethanol (Panreac) (see Scheme 1). SiC pellets were fabricated using commercially available SiC powders (200-450 mesh particle size, Aldrich, see further details on the Experimental section). Laser

ablation of the SiC pellet was performed using a Q-Switched Nd:YAG laser system (Rofin-Sinar Model PowerLine-E 20, Germany) emitting at 1064 nm to irradiate the target surface at a scan rate of 10 mm s^{-1}, a nominal laser power of 6.8 W in continuous mode (cw) operation, resulting in an irradiance value of 2.1 MW cm^{-2}. A homogeneous grayish colloidal suspension was obtained after 5 minutes of irradiation in ethanol. In contrast, larger aggregates were observed in the presence of water. Both solutions were directly evaluated by fluorescence spectroscopy and photo-luminescence (PL) was only observed in the ethanol-based solution. An additional centrifugation cycle to remove potential quenchers in the form of large aggregates did not render any significant change in the PL emission intensity of the particles synthesized in water solution. TEM images further confirmed the presence of large aggregates with a scarce number of nanoparticles even after size selection processes (see Figure S2 in the SI).

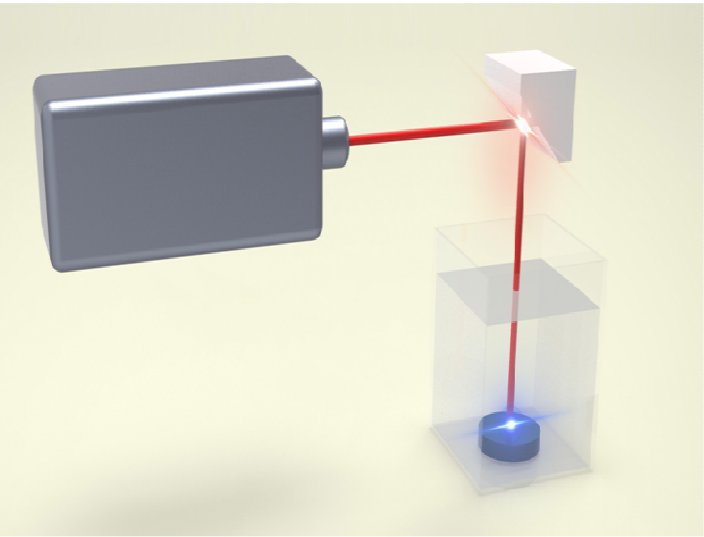

Scheme 1. Schematic sketch of the laser ablation experimental setup including the continuous mode laser source, the pelletized SiC target and a container for the liquid solvent.

In contrast, a homogeneous and clear solution containing small nanoparticles with a narrow size distribution of 2.1 ± 0.5 nm was obtained in the presence of ethanol. Figure 1 (a) displays a representative TEM image of the as-prepared SiC NPs obtained after laser ablation in ethanol and their nearly spherical morphology. A closer look provided by HRTEM shows fringe spacings of 0.26 nm, in good agreement with the (101) planes of bulk 6H-SiC, where a = 0.3081 nm and c = 1.5092 nm (JCPDS Card No. 29-1128). The corresponding PL emission spectra of the solution are shown in Fig. 1d. The monotonic red-shift of the PL maxima and the progressive drop in emission intensities with increasing excitation wavelengths can be attributed to quantum confinement effects and different particle size distributions. PL intensity maxima centered at 380 nm are obtained at an excitation wavelength of 240 nm. This broad ultraviolet PL peak has been previously reported for small and purified SiC NPs synthesized by electrochemical anodization of hexagonal [26] or cubic SiC wafers [25]. The observed blue-shift relative to the bulk 6H-SiC (band gap: ~ 406.5 nm) further corroborates the existence of energy subbands in the nanocrystals and quantum confinement effects induced by the size reduction [2,27]. Nevertheless, additional spectroscopic techniques were employed to thoroughly evaluate the structure and composition of the SiC NPs (*vide infra*).

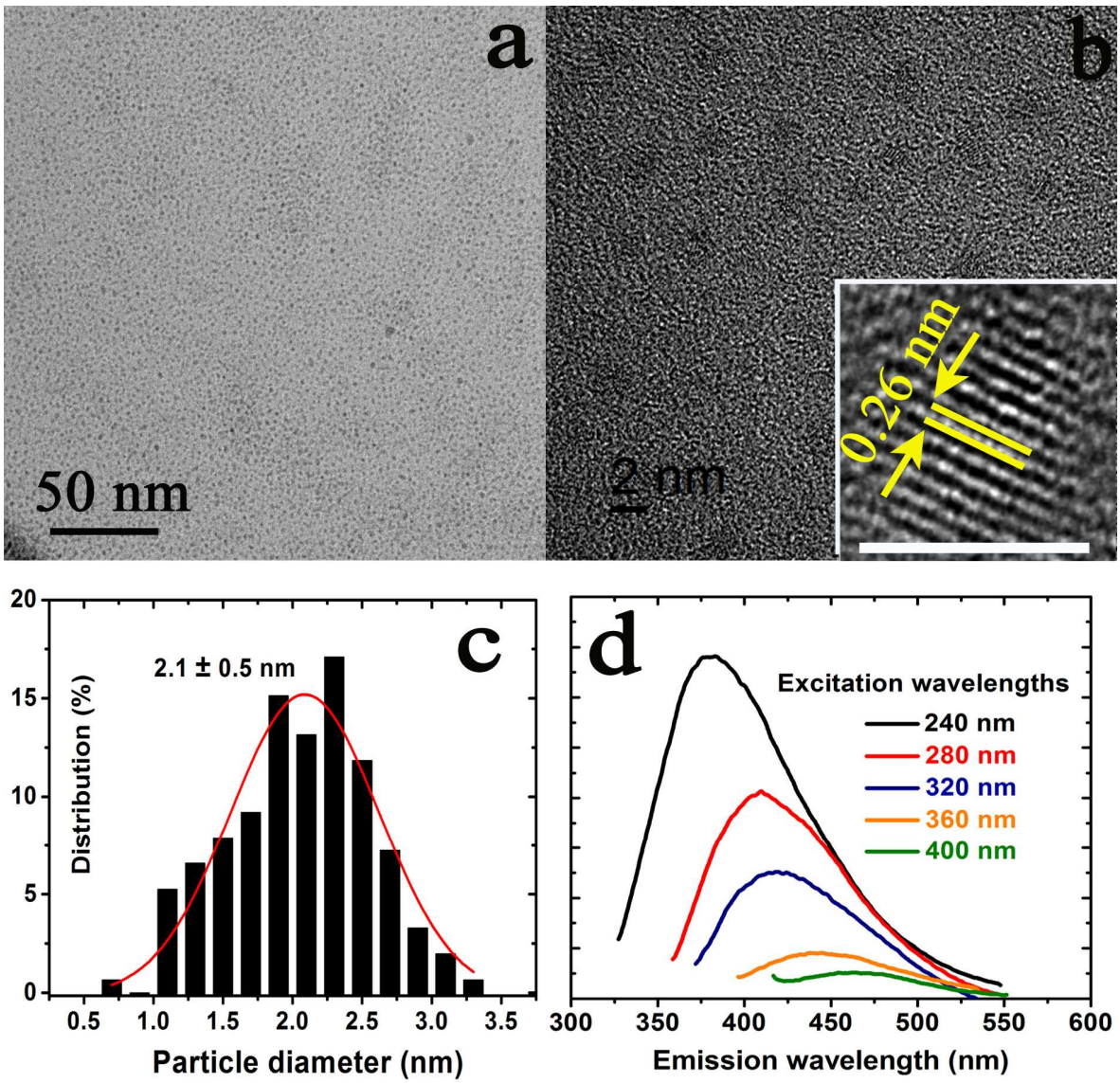

Figure 1: (a) Conventional TEM image showing a homogenous distribution of NP obtained after laser ablation in the presence of ethanol and deposited on an amorphous carbon film; (b) High-magnification TEM micrograph of one of these areas where those NP are clearly visible; (inset: HRTEM image of an individual NP with lattice fringes attributable to the (101) planes of 6H-SiC); (c) Particle size distribution of the SiC NPs obtained in the ethanolic dispersion; (d) Photoluminescence Emission spectra of SiC NPs corresponding to different excitation wavelengths.

Additional spectroscopic characterization of the luminescent SiC nanocrystals synthesized in the presence of ethanol. Spatial-resolved EELS is a powerful characterization technique in materials science because it allows the possibility of combining high-resolution imaging and spectroscopy, even at the atomic level [28-31]. An EELS spectrum-line (SPLI) has been recorded following the yellow line marked in the high angle annular dark field STEM image, inset of Figure 2a. We have selected 3 different EEL spectra, two of them corresponding to the sum of 3 consecutive EEL spectra recorded on the areas marked with a blue and a green arrow (corresponding to the blue (i) and green (ii) spectra), respectively, and a third one, in red (noted as (iii)), recorded in another similar particle of larger diameter (~ 6 nm), see Figure 2a. Characteristic signals corresponding to Si-$L_{2,3}$, C-K, and O-K edges, respectively, are visible in all these 3 EEL spectra.

The study of the energy loss near edge structure (ELNES) [28-31] provides very rich chemical bonding information at the subnanometer/atomic scale. Thus, the chemical bonding of Si was obtained by comparing the background substracted ELNES of the Si–$L_{2,3}$ edge in the 3 EEL selected spectra (see Figure 2b). Two mean peaks are observed at ~ 108 and ~114 eV, respectively. These two dominant peaks are associated to Si–O bonds like those in SiO_2 [32-33]. However, in the green (ii) and mainly in the blue (i) EEL spectra, a prominent shoulder at about 106 eV is observed and associated with Si–C bonds [32-34]. In fact, this signal stems from an overlapping effect caused by a simultaneous signal of these two compounds. It is also important to note that the C–K edge is mainly dominated by the signature of the amorphous carbon of the film supporting the NP.

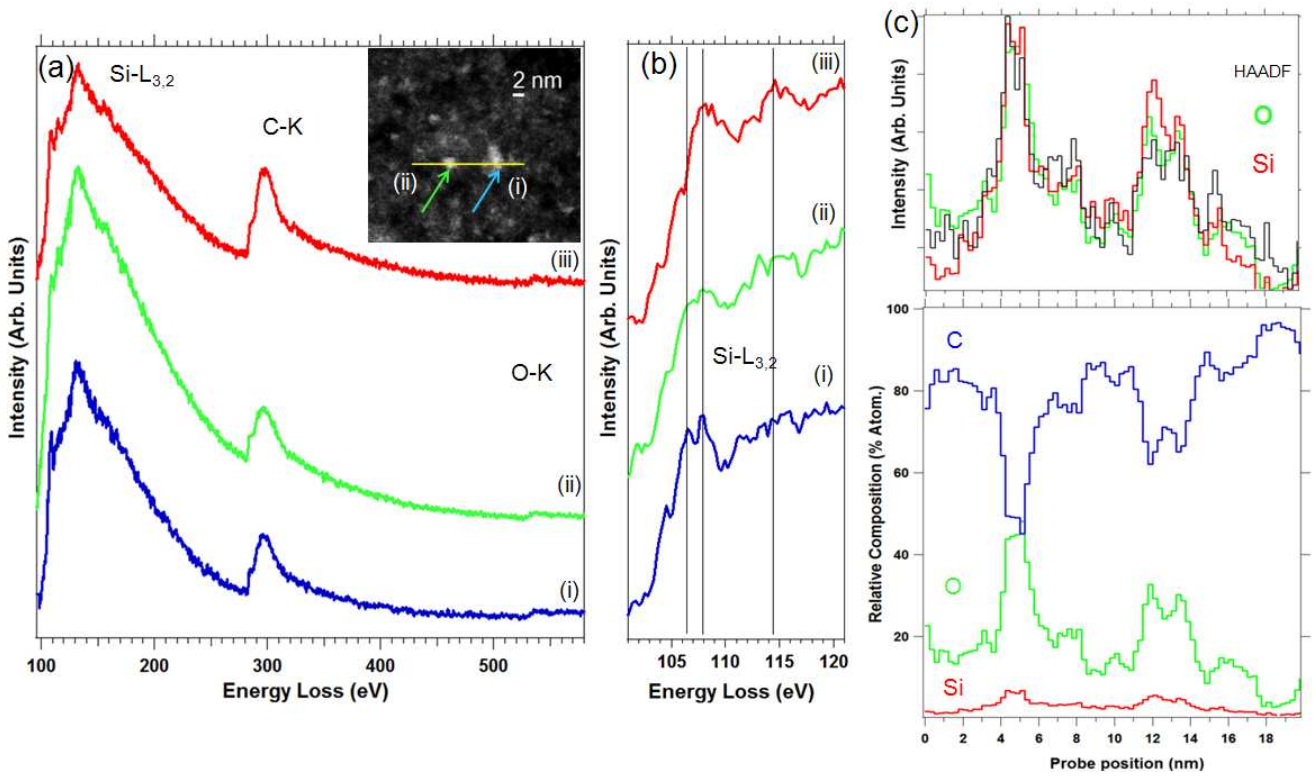

Figure 2: (a) EEL spectra sum of 3 EEL spectra extracted from the spectrum-line recorded in the yellow line marked in the inset of the STEM-HAADF image; (b) ELNES of the Si- $L_{2,3}$ edge for the 3 EEL spectra displayed in (a), see the text. (c) At the top: Si and O compared to HAADF intensity profile. At the bottom: relative composition (ato. %) of silicon, carbon and oxygen, obtained after background subtraction and quantitative analyses carried on the EELS-SPLI of Figure 2 (a) on Si-$L_{2,3}$, C-K and O-K edges, respectively.

The relative composition of each of these elements was obtained using standard quantifying procedures [30] on the EELS spectra extracted from the SPLI, see Figure 2c. From the compositional profiles of these elements as a function of the probe position, we can observe that, the Si and O contents are correlated where we plot simultaneously, Si and O atomic distribution with the intensity profile HAADF image) and anti-correlated to this one of C (see Figure 1 (f) at the bottom). This is due to the fact that these NP have been deposited in an amorphous C

membrane. From all these local analyses we can conclude that these NP are composed of SiC and covered by a layer of silicon oxide. Nevertheless, the presence of a complex Si-O-C compound [35] can not be ruled out at least at the surface of the NP. It is worth mentioning that all these results confirm those observed on these samples by macroscopic spectroscopic measurements, as discussed below (*vide infra*).

The surface composition of the SiC nanocrystals was also investigated by XPS and ATR. The Si 2p photoemission spectrum shown in Fig. 3(a) reveals a dominant contribution at 100.4 eV consistent with Si-C bonding energies [8,10-11,36]. After the spectrum was fit to the $Si2p_{3/2}$ and $Si2p_{1/2}$ spin-orbit partner lines, a low-intensity shoulder remained at higher binding energy and centered at 102.4 eV. This feature has been previously assigned to mixed suboxides [8,36]. Alternatively, other authors have proposed the formation of hydroxides (Si-OH) due to the interaction between the nanocrystal surfaces and the interacting molecules of the alcohol solvent as it is our case [5-6]. In the C1s spectrum, the strongest peak at 282.5 eV further corroborates the C-Si dominant component of the NCs surface (see Figure 3 (b)).

The ATR spectrum in Fig. 3(c) mainly shows the SiC transverse optical phonon vibration [4-6] at ca. 810 cm^{-1} and a broader band at ca. 1000 cm^{-1} that can be ascribed to Si-O-Si stretching vibrations. This partial surface oxidation can be associated to condensation and oxidation events between adjacent Si-OH terminations as previously discussed for Si NPs and also corroborated by the absence of O-H stretching modes in the 3000-3400 cm^{-1} region [20]. Raman spectroscopy is also a very useful technique for the observation of the quantum size effects in nanometer-sized particles and the structural characterization of nanomaterials. The Raman spectrum (Figure 3d) shows a well-defined peak at 781 cm^{-1} attributed to the 6H-SiC E_2 phonon mode and a non-well

resolved pre-peak at 768 cm^{-1} associated to the E_1 phonon mode[14]. The peak at 968 cm^{-1} is related to a longitudinal optical (LO) vibration mode [4,14]. Moreover, the absence of Si-Si contributions at 520 cm^{-1} further suggests the preferential formation of the silicon carbide structure of the nanoparticles.

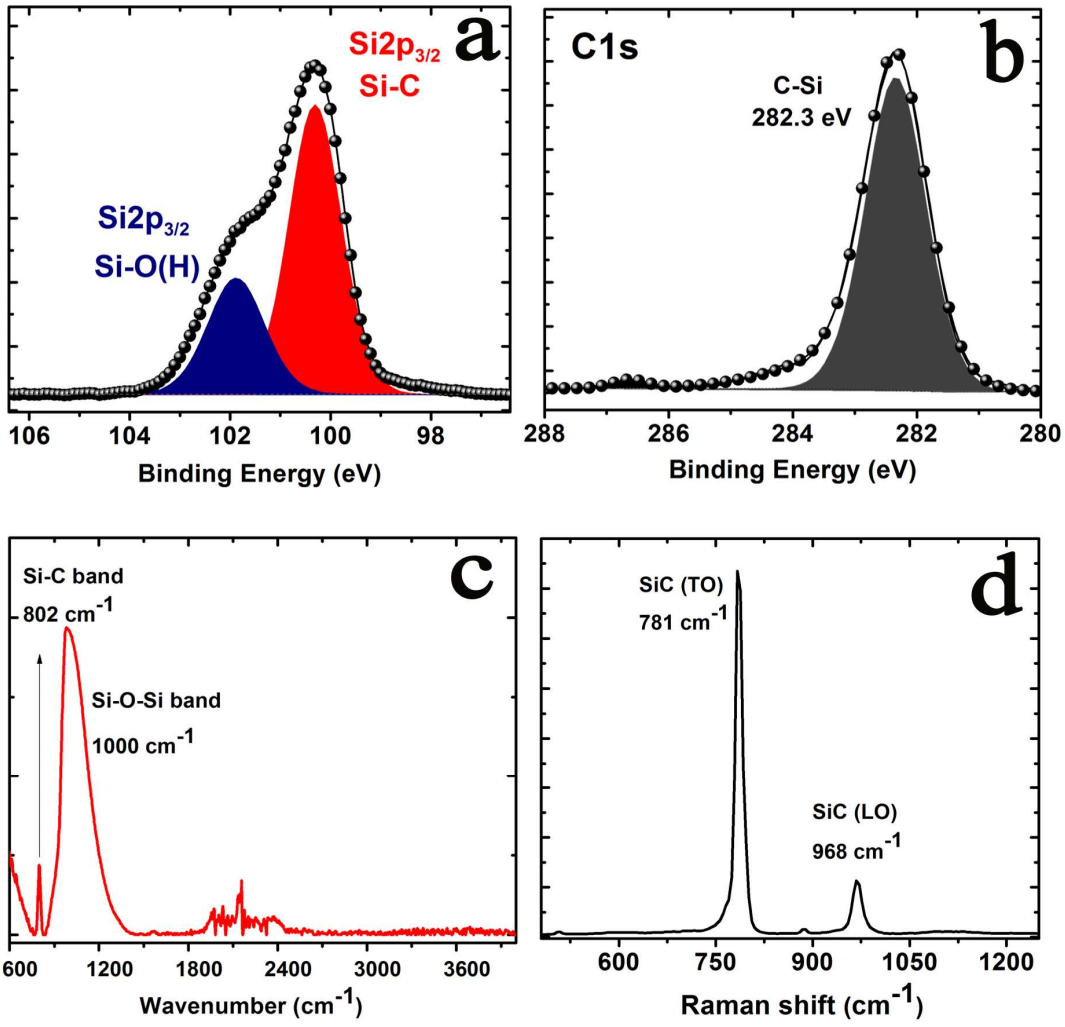

Figure 3. Additional spectroscopic characterization of the luminescent SiC NPs obtained after laser ablation in the presence of liquid ethanol: (a) X-ray Photoemission spectrum of the Si2p region; (b) XP spectrum corresponding to the C1s region; (c) Infrared absorption spectrum and (d) Raman spectrum. The measurements were carried out after solvent evaporation.

Ablation mechanisms and effect of solvents. Figure 4 outlines the synthetic approach to produce SiC NPs by laser ablation of pelletized micropowders and the reaction mechanisms that are taking place in the presence of an ethanolic liquid solution and in comparison with an aqueous solvent.

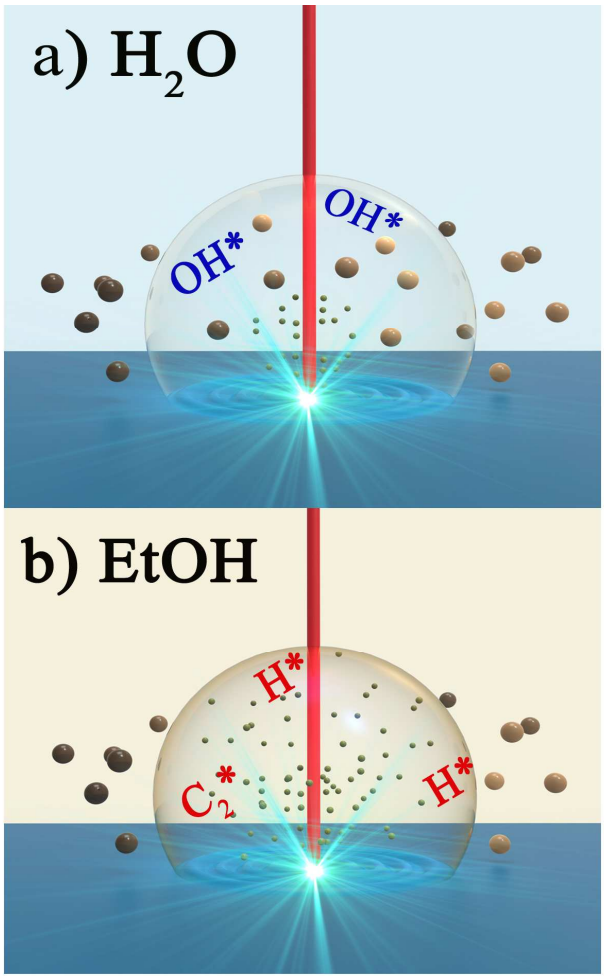

Figure 4. Schematic representation of the ablation process at the interface of the ablated SiC pellet and influence of the different reactive intermediates generated with the plasma cavity depending on the selected collecting solvent: a) hydroxyl and oxidizing radicals tend to passivate the surface and form larger amorphous SiOx particles; b) the reducing intermediates generated in the ethanol plasma prevent further oxidation of the ablated nanoparticles and favor a higher bubbling and etching rate.

Fabrication of NPs is a very complex process that may involve a wide variety of phenomena. Formation of NPs may take place through several mechanisms which are largely driven by the laser irradiation conditions imposed. These include essentially the emission wavelength, the laser operation mode (cw or pulsed), the irradiance level (where interaction times are implicit, expressed in Wcm^{-2}) and the pulse repetition rate (which may cause an effect known as incubation). Nucleation and growth may take place within the plasma plume, according to some authors, where the presence of excited intermediates and clusters is a trademark [37-38]. After the occurrence of the plasma, the initial layer of molten material above the surface of the target in combination with mechanical shock waves generated by the plasma plume may promote ejection of molten droplets, as well as solid fragments from the surface.

Moreover, since LASiS takes place in a liquid medium, other contributions to this interaction mechanism must be taken into account. Although some authors have demonstrated the usefulness of direct cw nIR laser irradiation towards achieving controlled synthesis of nanotubes, nanofoams and other nanostructures [39-40] most published works on laser synthesis within a liquid medium have made use of pulsed laser irradiation. In the present work, a laser with cw emission is used to induce the ablation process within the liquid medium. Heating of the liquid medium is thus expected. The energy is released on a time scale much larger than the electron-phonon relaxation time and material detachment occurs by thermal ablation mechanisms as follows. Initially, the target irradiated melts within the laser spot and forms a vapor plume, as a result of continued laser irradiation. The vapor plume turns into a plasma plume upon further irradiation [37] as the laser irradiance level is above 10^4 W cm^{-2} so that photothermal ablation governs the NPs generation mechanism [38].

In photothermal ablation the shock wave that accompanies the laser irradiation may have two different contributions. One is due to the high-pressure gradients that the excited species generate within the plasma plume; the other is the mechanical shockwave produced by the material ablated from the surface [37]. These mechanisms are enhanced when the laser irradiation occurs within liquid media, since the plasma is confined and the mechanical shockwave is even more intense [41]. The solvent properties are also critical for this method since, for instance, no luminescence effect has been observed in particles generated in water. The ablation process seems to be less efficient since the corresponding energy contribution from the solvent is practically negligible. Water acts as an efficient cooling agent, further contributing to significantly lower the ablation rate of the target. Its latent heat of vaporization (~ 2270 $kJ \cdot kg^{-1}$) and specific heat capacity (4.187 $kJ \cdot kg^{-1} \cdot K^{-1}$) values are relatively high due to the presence of strong hydrogen bonds and have been previously defined as influencing parameters in the rate of bubble generation to remove the detached material [41-42]. Likewise, bubbling rate has been addressed as an influencing parameter in the etching rate of materials immersed in water [41] and can partly justify the minimal presence of individual nanoparticles when the laser ablation process was carried out in the aqueous phase (see SI).

On the other hand, organic solvents such as ethanol typically have lower boiling temperatures, heat capacities (~ 2.46 $kJ \cdot kg^{-1} \cdot K^{-1}$) and heat of vaporization values (~ 855 $kJ \cdot kg^{-1}$) that affect to a lower extent to the local heating at the solid-liquid interface during the *cw* laser ablation scans. In addition, ethanol prevents the total oxidation of the particles, favoring a generation process closer to the laser pyrolysis mechanisms observed by other authors in non reactive [39-40,43] and organic atmospheres [41,44-45]. Under our experimental conditions, the more efficient

ablation mechanism observed using ethanol probably facilitated the narrowing down of a higher fraction of microsized particles already in suspension after multiple laser irradiation sweeps [41,46-47]. Smaller size particles may also appear, in addition, apparently related to target vaporization at the laser focus, followed by condensation phenomena [47]. The higher fraction of stable nanoparticles obtained in ethanol and the absence of luminescence in the suspension in the presence of water must be also explained in terms of the laser chemistry derived from the different excited intermediates generated within the plasma plume and the solvent molecules [41]. Plasma confined within the liquid media is able to enhance the action of laser irradiation[41]. Thus, a combination of reactive species is obtained due to the partial excitation, ionization and/or dissociation of molecules from the solvent that would be otherwise neutral at room temperature. These intermediates will likely interact with the ablated material and will further react with the liquid molecules after the shock-wave propagation induced by the plasma expansion step [41-42].

Optical emission spectroscopy (OES) has previously determined that the plasma chemistry of water generates a vast amount of highly reactive hydroxyl radicals stemming from water molecules dissociation with probed oxidative capacity [41,48-49]. Likewise, other authors have demonstrated experimentally the generation of an interfacial region where highly excited ablated species modify the properties of organic solvents and induce the formation of C* and H* excited intermediates [41,47-50]. The presence of this latter reductive atmosphere can explain why the small nanoparticles collected in ethanol appear only slightly oxidized in their outer surface and retain their photoluminescence properties. The oxidation processes may be taking place during the re-solidification of molten material ejected from the target. It can be also associated to the

formation of defects on particles generated after rapid solidification. Nevertheless, the presence of surface oxidized states does not prevent the PL emission properties of SiC quantum dots as previously reported in numerous works. In contrast, the oxidative atmosphere generated in the presence of water excited intermediates in conjunction with a lower ablation rate can justify the total oxidation of the target surface during the ablation process, the induction of a major formation of Si-OH and $Si-O^-$ bonds in the ablated materials containing defects and the lack of colloidal stability observed after several hours induced by the aggregation of the ablated particles present in the aqueous suspension. All these fact undoubtedly led to the absence of stable and luminescent nanoparticles.

In summary, this paper reports on the direct and cost-effective synthesis of ultra-small and luminescent SiC NPs by laser ablation in the presence of liquid ethanol. We have proposed the use of inexpensive SiC commercial micropowders that can be compressed and pelletized as targets for the laser ablation reaction. Although the use of powdered targets has been previously proposed for the deposition of SiC thin films or in colloidal reaction involving strong acid solutions, it has not been proposed before for direct synthesis of SiC NPs slightly oxidized in their outer surface by LASiS. Herein, we have successfully overcome several shortcomings: i) the handling of toxic reactants; ii) the use of expensive and time-consuming wafers (difficult to handle and prepare); iii) minimized the formation of multiple silicon phases since we already have a pre-defined SiC crystalline phase. These nanoparticles, thus, exhibit a tremendous potential as functional nanomaterials for multidisciplinary applications.

Experimental Methods

Synthesis. The SiC NPs were fabricated by laser ablation of pelletized SiC powders previously immersed in a glass vessel with 10 mL of absolute ethanol (Panreac). SiC pellets were fabricated using commercially available SiC powders (200-450 mesh particle size, Aldrich). This SiC powder was ground with an agate mortar and mixed with an organic ligand (Poly(vinylidene fluoride) from Fluka) in a 2 % weight to facilitate the integration in a pelletized configuration. After compacting, the ligand was removed at 250 ºC and a final target with 13 mm diameter and 1.9 mm thickness was obtained. Laser ablation of the SiC pellet was performed using a Q-Switched Nd:YAG laser system (Rofin-Sinar Model PowerLine-E 20, Germany) emitting at 1064 nm to irradiate the target surface at a scan rate of 10 mm s^{-1}, a nominal laser power of 6,8 W in continuous mode (cw) operation, resulting in an irradiance value of 2.1 MW cm^{-2}. During laser ablation, the target was automatically shifted using a rectangular focal plane to achieve more uniform irradiation of the SiC surface. Finally, a homogeneous grayish colloidal suspension was obtained after 5 minutes of irradiation. After a centrifugation cycle to remove larger particles, a transparent and stable solution containing SiC nanoparticles was obtained.

Characterization techniques. PL spectra were acquired with an LS55 Fluorescence Spectrometer (PerkinElmer) equipped with a Xenon arc lamp as the light source and a quartz cell (1 x 1 cm). The surface composition was analyzed by Fourier transform infrared (FTIR) spectroscopy using a Bruker Vertex 70 FTIR spectrometer and by X-ray photoelectron spectroscopy (XPS) with an Axis Ultra DLD (Kratos Tech.). The size distribution of each sample was obtained through statistics over 120 particles. All measurements were performed at room temperature. The as-obtained samples were also studied by transmission electron microscopy (TEM). Conventional TEM and high-resolution (HRTEM) studies were performed on a FEI

Tecnai (operating at 200KV) and on an imaging-side aberration-corrected FEI Titan-Cube microscope working at 80 kV, equipped with a Cs corrector (CETCOR from CEOS GmbH), respectively. Atomic-resolved electron energy loss spectroscopy (EELS) measurements, as well as scanning TEM (STEM) studies were performed on probe-corrected STEM FEI Titan Low-Base 60-300 operating at 80KV (fitted with a X-FEG gun and Cs-probe corrector (CESCOR from CEOS GmbH)). EEL spectra were recorded using the spectrum-imaging mode [a] in a Gatan GIF Tridiem ESR spectrometer. The convergent semi-angle was of 25 mrad, the collection semi-angle was of 50 mrad and the energy resolution ~ 1.1 eV.

ASSOCIATED CONTENT

Supporting Information. SEM and TEM images of the original microsized SiC precursor material and TEM images of the particles obtained after laser ablation in water. This material is available free of charge via the Internet at http://pubs.acs.org.

AUTHOR INFORMATION

***Corresponding Author: Prof. Germán de la Fuente**

*Email: xerman@unizar.es; Phone:(+34) 976762527

***Corresponding Author: Dr. José L. Hueso**

*Email: jlhueso@unizar.es; Phone : (+34)876555442

The authors declare no competing financial interests.

ACKNOWLEDGMENTS

The research leading to these results has received funding from the People Program (under Marie Curie Grant agreement 294094-NANOLIGHT). R.A. acknowledges funding from the Spanish Ministerio de Economia y Competitividad (FIS2013-46159-C3-3-P) and from the European Comission under Graphene Flagship (contract no. CNECT-ICT-604391) and under Grant Agreement 312483 - ESTEEM2 (Integrated Infrastructure Initiative - I3). Additional funding from 314630 – UV Marking (FoF) and DGA (Laser Applications Lab, T87) is also gratefully acknowledged. JLH thanks for a Juan de la Cierva Postdoctoral Fellowship from the Spanish Ministry of Science and Education. The TEM measurements were performed in the Laboratorio de Microscopias Avanzadas (LMA) at the Instituto de Nanociencia de Aragon (INA) - Universidad de Zaragoza (Spain).

REFERENCES

[1] Fan, J. Y.; Chu, P. K., Group IV Nanoparticles: Synthesis, Properties, and Biological Applications. *Small* **2010,** *6* (19), 2080-2098.

[2] Fan, J. Y.; Li, H. X.; Wang, J.; Xiao, M., Fabrication and photoluminescence of SiC quantum dots stemming from 3C, 6H, and 4H polytypes of bulk SiC. *Appl. Phys. Lett.* **2012,** *101* (13).

[3] Fan, J. Y.; Wu, X. L.; Li, H. X.; Liu, H. W.; Siu, G. G.; Chu, P. K., Luminescence from colloidal 3C-SiC nanocrystals in different solvents. *Appl. Phys. Lett.* **2006,** *88* (4).

[4] Beke, D.; Szekrenyes, Z.; Balogh, I.; Veres, M.; Fazakas, E.; Varga, L. K.; Kamaras, K.; Czigany, Z.; Gali, A., Characterization of luminescent silicon carbide nanocrystals prepared by reactive bonding and subsequent wet chemical etching. *Appl. Phys. Lett.* **2011,** *99* (21).

[5] Wang, J.; Xiong, S. J.; Wu, X. L.; Li, T. H.; Chu, P. K., Glycerol-Bonded 3C-SiC Nanocrystal Solid Films Exhibiting Broad and Stable Violet to Blue-Green Emission. *Nano Lett.* **2010,** *10* (4), 1466-1471.

[6] Wu, X. L.; Xiong, S. J.; Zhu, J.; Wang, J.; Shen, J. C.; Chu, P. K., Identification of Surface Structures on 3C-SiC Nanocrystals with Hydrogen and Hydroxyl Bonding by Photoluminescence. *Nano Lett.* **2009,** *9* (12), 4053-4060.

[7] Botsoa, J.; Lysenko, V.; Geloen, A.; Marty, O.; Bluet, J. M.; Guillot, G., Application of 3C-SiC quantum dots for living cell imaging. *Appl. Phys. Lett.* **2008,** *92* (17).

[8] Hessel, C. M.; Rasch, M. R.; Hueso, J. L.; Goodfellow, B. W.; Akhavan, V. A.; Puvanakrishnan, P.; Tunnel, J. W.; Korgel, B. A., Alkyl Passivation and Amphiphilic Polymer Coating of Silicon Nanocrystals for Diagnostic Imaging. *Small* **2010,** *6* (18), 2026-2034.

[9] Fan, J.; Chu, P. K., Group IV Nanoparticles: Synthesis, Properties, and Biological Applications. *Small* **2010,** *6* (19), 2080-2098.

[10] Dasog, M.; Smith, L. F.; Purkait, T. K.; Veinot, J. G. C., Low temperature synthesis of silicon carbide nanomaterials using a solid-state method. *Chem. Commun.* **2013,** *49* (62), 7004-7006.

[11] Henderson, E. J.; Veinot, J. G. C., From Phenylsiloxane Polymer Composition to Size-Controlled Silicon Carbide Nanocrystals. *J. Am. Chem. Soc.* **2009,** *131* (2), 809-815.

[12] Donato, A.; Borsella, E.; Botti, S.; Martelli, S.; Nannetti, C. A.; Mancini, M. R.; Morjan, I., Thermal shock tests of beta-sic pellets prepared from laser synthesized nanoscale sic powders. *J. Nucl. Mater.* **1996,** *233*, 814-817.

[13] Herlin-Boime, N.; Vicens, J.; Dufour, C.; Tenegal, F.; Reynaud, C.; Rizk, R., Flame temperature effect on the structure of SiC nanoparticles grown by laser pyrolysis. *J. Nanopart. Res.* **2004,** *6* (1), 63-70.

[14] Quinones-Galvan, J. G.; Arias-Ceron, J. S.; de Moure-Flores, F., Stoichiometric 6H-SiC thin films deposited at low substrate temperature by laser ablation. *J. Laser Appl.* **2013,** *25* (5).

[15] Miotello, A.; Kelly, R., Laser-induced phase explosion: new physical problems when a condensed phase approaches the thermodynamic critical temperature. *Appl. Phys. A-Mater. Sci. Process.* **1999,** *69*, S67-S73.

[16] Amendola, V.; Meneghetti, M., What controls the composition and the structure of nanomaterials generated by laser ablation in liquid solution? *Phys. Chem. Chem. Phys.* **2013,** *15* (9), 3027-3046.

[17] Malumbres, A.; Martinez, G.; Mallada, R.; Hueso, J. L.; Bomati-Miguel, O.; Santamaria, J., Continuous production of iron-based nanocrystals by laser pyrolysis. Effect of operating variables on size, composition and magnetic response. *Nanotechnology* **2013,** *24* (32).

[18] Martinez, G.; Malumbres, A.; Mallada, R.; Hueso, J. L.; Irusta, S.; Bomati-Miguel, O.; Santamaria, J., Use of a polyol liquid collection medium to obtain ultrasmall magnetic nanoparticles by laser pyrolysis. *Nanotechnology* **2012,** *23* (42).

[19] Intartaglia, R.; Bagga, K.; Genovese, A.; Athanassiou, A.; Cingolani, R.; Diaspro, A.; Brandi, F., Influence of organic solvent on optical and structural properties of ultra-small silicon dots synthesized by UV laser ablation in liquid. *Phys. Chem. Chem. Phys.* **2012,** *14* (44), 15406-15411.

[20] Svrcek, V.; Mariotti, D.; Nagai, T.; Shibata, Y.; Turkevych, I.; Kondo, M., Photovoltaic Applications of Silicon Nanocrystal Based Nanostructures Induced by Nanosecond Laser Fragmentation in Liquid Media. *J. Phys. Chem. C* **2011,** *115* (12), 5084-5093.

[21] Abderrafi, K.; Calzada, R. G.; Gongalsky, M. B.; Suarez, I.; Abarques, R.; Chirvony, V. S.; Timoshenko, V. Y.; Ibanez, R.; Martinez-Pastor, J. P., Silicon Nanocrystals Produced by Nanosecond Laser Ablation in an Organic Liquid. *J. Phys. Chem. C* **2011,** *115* (12), 5147-5151.

[22] Liu, P.; Cui, H.; Wang, C. X.; Yang, G. W., From nanocrystal synthesis to functional nanostructure fabrication: laser ablation in liquid. *Phys. Chem. Chem. Phys.* **2010,** *12* (16), 3942-3952.

[23] Zakharko, Y.; Rioux, D.; Patskovsky, S.; Lysenko, V.; Marty, O.; Bluet, J. M.; Meunier, M., Direct synthesis of luminescent SiC quantum dots in water by laser ablation. *Phys. Status Solidi-Rapid Res. Lett.* **2011,** *5* (8), 292-294.

[24] Yan, Z. J.; Chrisey, D. B., Pulsed laser ablation in liquid for micro-/nanostructure generation. *J. Photochem. Photobiol. C-Photochem. Rev.* **2012,** *13* (3), 204-223.

[25] Yang, S. K.; Cai, W. P.; Zeng, H. B.; Xu, X. X., Ultra-fine beta-SiC quantum dots fabricated by laser ablation in reactive liquid at room temperature and their violet emission. *J. Mater. Chem.* **2009,** *19* (38), 7119-7123.

[26] Botsoa, J.; Bluet, J. M.; Lysenko, V.; Sfaxi, L.; Zakharko, Y.; Marty, O.; Guillot, G., Luminescence mechanisms in 6H-SiC nanocrystals. *Phys. Rev. B* **2009,** *80* (15).

[27] Rossi, A. M.; Murphy, T. E.; Reipa, V., Ultraviolet photoluminescence from 6H silicon carbide nanoparticles. *Appl. Phys. Lett.* **2008,** *92* (25).

[28] Arenal, R.; Blase, X.; Loiseau, A., Boron-nitride and boron-carbonitride nanotubes: synthesis, characterization and theory. *Adv. Phys.* **2010,** *59* (2), 101-179.

[29] Arenal, R.; de la Pena, F.; Stephan, O.; Walls, M.; Tence, M.; Loiseau, A.; Colliex, C., Extending the analysis of EELS spectrum-imaging data, from elemental to bond mapping in complex nanostructures. *Ultramicroscopy* **2008,** *109* (1), 32-38.

[30] Egerton, R., *Electron Energy-Loss Spectroscopy in the Electron Microscope*. Springer: 2011.

[31] Pennycook, S. J.; Nellist, P. D., Scanning Transmission Electron Microscopy: Imaging and Analysis. Springer Science & Business Media: 2011.

[32] Garvie, L. A. J.; Buseck, P. R., Bonding in silicates: Investigation of the Si L-2,L-3 edge by parallel electron energy-loss spectroscopy. *Am. Miner.* **1999,** *84* (5-6), 946-964.

[33] Pippel, E.; Lichtenberger, O.; Woltersdorf, J., Identification of silicon oxycarbide bonding in Si-C-O-glasses by EELS. *J. Mater. Sci. Lett.* **2000,** *19* (22), 2059-2060.

[34] Pippel, E.; Woltersdorf, J.; Olafsson, H. O.; Sveinbjornsson, E. O., Interfaces between 4H-SiC and SiO2: Microstructure, nanochemistry, and near-interface traps. *J. Appl. Phys.* **2005,** *97* (3).

[35] Mazo, M. A.; Tamayo, A.; Rubio, F.; Soriano, D.; Rubio, J., Effect of processing on the structural characteristics of sintered silicon oxycarbide materials. *J. Non-Cryst. Solids* **2014,** *391*, 23-31.

[36] Hessel, C. M.; Reid, D.; Panthani, M. G.; Rasch, M. R.; Goodfellow, B. W.; Wei, J. W.; Fujii, H.; Akhavan, V.; Korgel, B. A., Synthesis of Ligand-Stabilized Silicon Nanocrystals with Size-Dependent Photoluminescence Spanning Visible to Near-Infrared Wavelengths. *Chem. Mat.* **2012,** *24* (2), 393-401.

[37] Bäuerle, D. W., *Laser Processing and Chemistry*. Springer: 2011.

[38] Rubahn, H. G., *Laser Applications in Surface Science and Technology*. Wiley: 1999.

[39] Munoz, E.; Ruiz-Gonzalez, M. L.; Seral-Ascaso, A.; Sanjuan, M. L.; Gonzalez-Calbet, J. M.; Laguna, M.; de la Fuente, G. F., Tailored production of nanostructured metal/carbon foam by laser ablation of selected organometallic precursors. *Carbon* **2010,** *48* (6), 1807-1814.

[40] Seral-Ascaso, A.; Garriga, R.; Sanjuan, M. L.; Razal, J. M.; Lahoz, R.; Laguna, M.; de la Fuente, G. F.; Munoz, E., 'Laser chemistry' synthesis, physicochemical properties, and chemical processing of nanostructured carbon foams. *Nanoscale Res. Lett.* **2013,** *8*.

[41] Kruusing, A., Underwater and water-assisted laser processing: Part 2 - Etching, cutting and rarely used methods. *Opt. Lasers Eng.* **2004,** *41* (2), 329-352.

[42] Ageev, V. A.; Bokhonov, A. F.; Zhukovskii, V. V.; Yankovskii, A. A., Formation of gas cavity under the laser metal ablation in liquid. *Publications of the Astronomical Observatory of Belgrade, No 53: Proceedings of the First Belarussian-Yugoslavian Symposium on Physics and*

Diagnostics of Laboratory & Astrophysical Plasma - in Memoriam of M. A. Elyashevich, Academician of Belarus As **1996**, 43-46.

[43] Garcia, M. A.; Ruiz-Gonzalez, M. L.; de la Fuente, G. F.; Crespo, P.; Gonzalez, J. M.; Llopis, J.; Gonzalez-Calbet, J. M.; Vallet-Regi, M.; Hernando, A., Ferromagnetism in twinned Pt nanoparticles obtained by laser ablation. *Chem. Mat.* **2007,** *19* (4), 889-893.

[44] Dolgaev, S. I.; Simakin, A. V.; Voronov, V. V.; Shafeev, G. A.; Bozon-Verduraz, F., Nanoparticles produced by laser ablation of solids in liquid environment. *Appl. Surf. Sci.* **2002,** *186* (1-4), 546-551.

[45] Shafeev, G. A.; Obraztsova, E. D.; Pimenov, S. M., Laser-assisted etching of diamonds in air and in liquid media. *Appl. Phys. A-Mater. Sci. Process.* **1997,** *65* (1), 29-32.

[46] Bosbach, J.; Martin, D.; Stietz, F.; Wenzel, T.; Trager, F., Laser-based method for fabricating monodisperse metallic nanoparticles. *Appl. Phys. Lett.* **1999,** *74* (18), 2605-2607.

[47] Sakka, T.; Iwanaga, S.; Ogata, Y. H.; Matsunawa, A.; Takemoto, T., Laser ablation at solid-liquid interfaces: An approach from optical emission spectra. *J. Chem. Phys.* **2000,** *112* (19), 8645-8653.

[48] Hueso, J. L.; Espinos, J. P.; Caballero, A.; Cotrino, J.; Gonzalez-Elipe, A. R., XPS investigation of the reaction of carbon with NO, O-2, N-2 and H2O plasmas. *Carbon* **2007,** *45* (1), 89-96.

[49] Hueso, J. L.; Rico, V. J.; Cotrino, J.; Jimenez-Mateos, J. M.; Gonzalez-Elipe, A. R., Water plasmas for the revalorisation of heavy oils and cokes from petroleum refining. *Environ. Sci. Technol.* **2009,** *43* (7), 2557-2562.

[50] Yanguas-Gil, A.; Hueso, J. L.; Cotrino, J.; Caballero, A.; Gonzalez-Elipe, A. R., Reforming of ethanol in a microwave surface-wave plasma discharge. *Appl. Phys. Lett.* **2004,** *85* (18), 4004-4006.

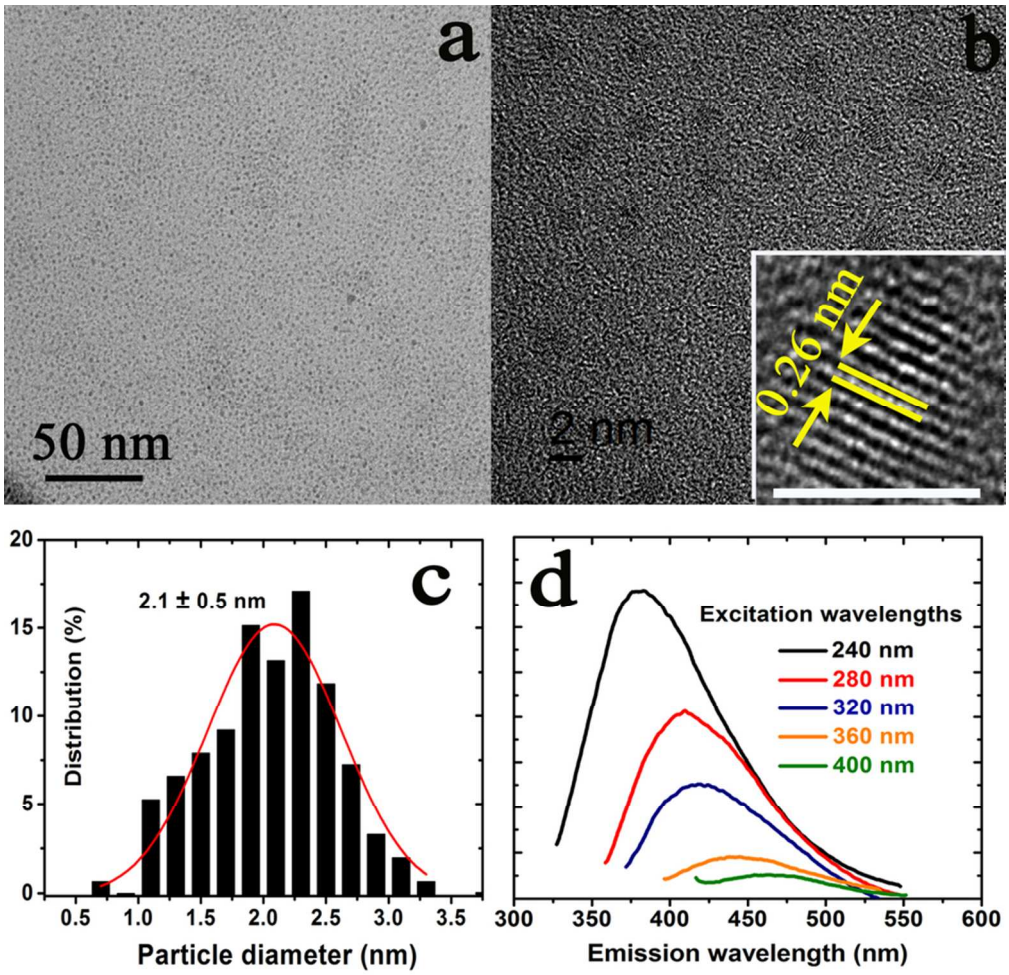

Figure 1
80x80mm (300 x 300 DPI)

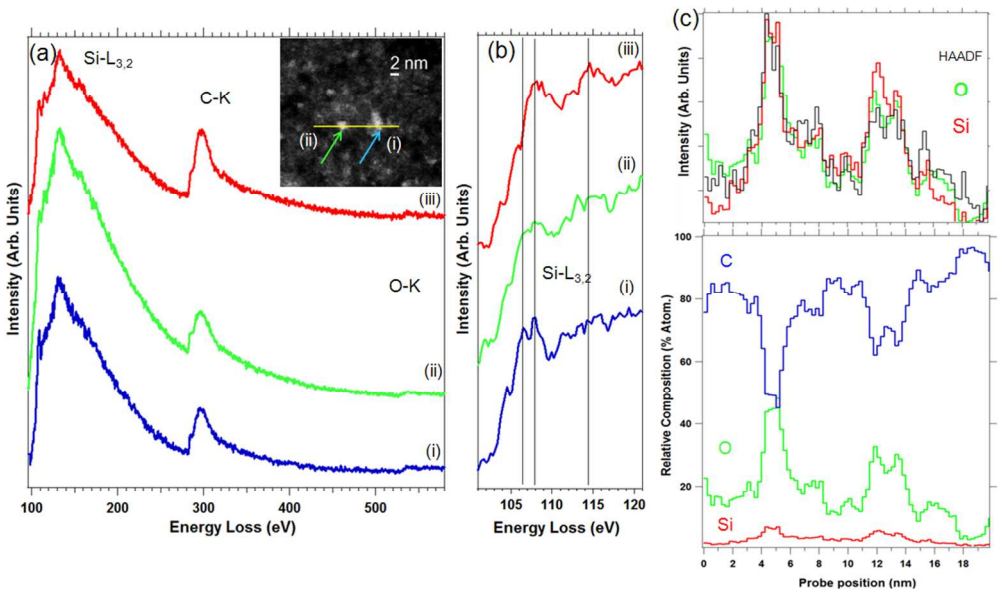

Figure 2
114x67mm (260 x 260 DPI)

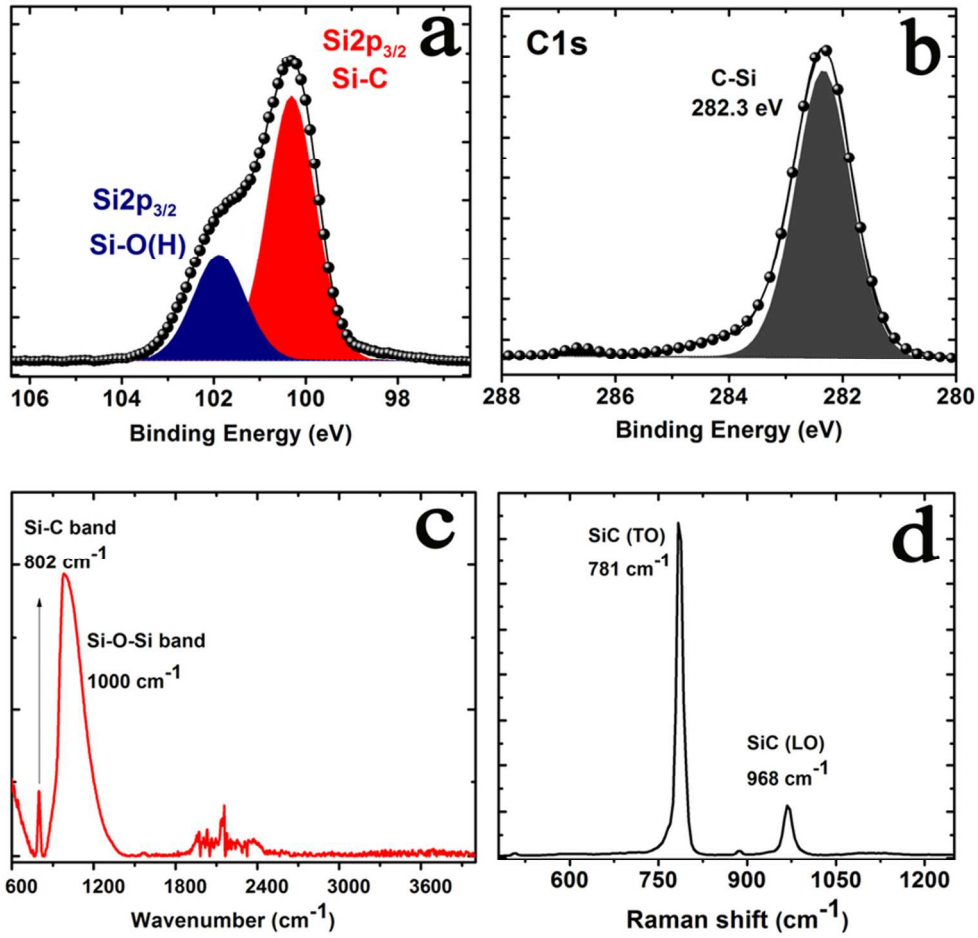

Figure 3
80x80mm (300 x 300 DPI)

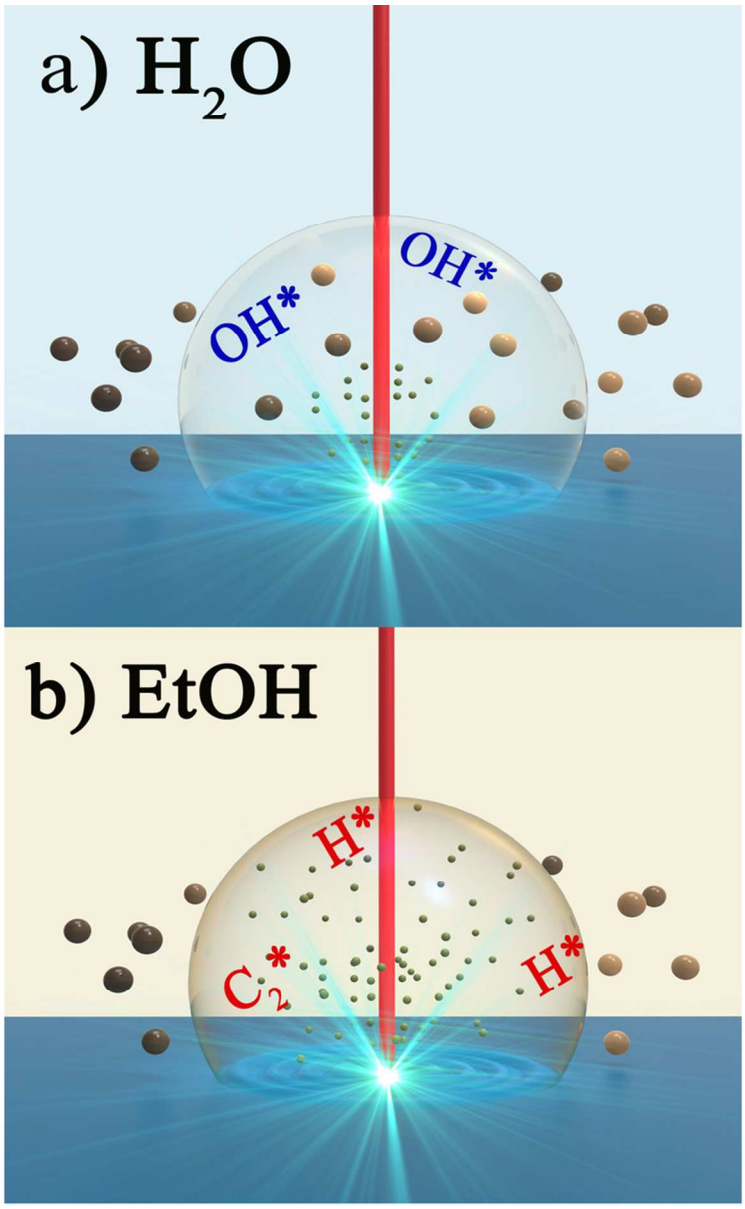

Figure 4
80x106mm (300 x 300 DPI)